The Chromophore Structures of the Pr States in Plant and Bacterial Phytochromes

Daniel H. Murgida,* David von Stetten,* Peter Hildebrandt,* Pascale Schwinté,[†] Friedrich Siebert,[†] Shivani Sharda,[‡] Wolfgang Gärtner,[‡] and Maria Andrea Mroginski*

*Technische Universität Berlin, Institut für Chemie, Max-Volmer-Laboratorium für Biophysikalische Chemie, Sekr. PC 14, D-10623 Berlin, Germany; [†]Universität Freiburg, Institut für Molekulare Medizin und Zellforschung, Sektion Biophysik, D-79104 Freiburg, Germany; and [‡]Max-Planck-Institut für Bioanorganische Chemie, D-45470 Mülheim, Germany

ABSTRACT   The resonance Raman spectra of the Pr state of the N-terminal 65-kDa fragment of plant phytochrome phyA have been measured and analyzed in terms of the configuration and conformation of the tetrapyrroles methine bridges. Spectra were obtained from phyA adducts reconstituted with the natural chromophore phytochromobilin as well as phycocyanobilin and its isotopomers labeled at the terminal methine bridges through $^{13}C/^{12}C$ and D/H substitution. Upon comparing the resonance Raman spectra of the various phyA adducts, it was possible to identify the bands that originate from normal modes dominated by the stretching coordinates of the terminal methine bridges *A-B* and *C-D*. Quantum chemical calculations of the isolated tetrapyrroles reveal that these modes are sensitive indicators for the methine bridge configuration and conformation. For all phyA adducts, the experimental spectra of Pr including this marker band region are well reproduced by the calculated spectra obtained for the *ZZZasa* configuration. In contrast, there are substantial discrepancies between the experimental spectra and the spectra calculated for the *ZZZssa* configuration, which has been previously shown to be the chromophore geometry in the Pr state of the bacterial, biliverdin-binding phytochrome from *Deinococcus radiodurans* (Wagner, J. R., J. S. Brunzelle, K. T. Forest, R. D. Vierstra. 2005. *Nature*. 438:325–331). The results of this work, therefore, suggest that plant and bacterial (biliverdin-binding) phytochromes exhibit different structures in the parent state although the mechanism of the photoinduced reaction cycle may be quite similar.

INTRODUCTION

Phytochromes constitute a family of plant photoreceptors that regulate a wide variety of photomorphogenic processes (1,2). They act as photochemical switches that interconvert between the inactive (Pr, red-absorbing form) and the active (Pfr, far-red-absorbing form) state of the receptor, thereby controlling the recognition by reaction partners of the downstream signaling processes (1–4). Despite extensive studies on phytochromes in the past decades, the understanding of the molecular mechanism of the light-induced activation is still at its infancy. No three-dimensional structure data are yet available on plant phytochromes, and the numerous spectroscopic studies have led to partially conflicting conclusions (2,5–7). In view of the serious difficulties to crystallize these proteins, bacterial representatives of this photoreceptor family have become alternative targets of molecular phytochrome research. Bacterial phytochromes share a number of similarities with their counterparts from plants, including the composition of the individual domains that involve the chromophore-binding GAF- (found in cGMP-specific phosphodiesterases) and PHY- (phytochrome) domains (5). These domains, and the very N-terminal part, which often folds into a Per-Arnt-Sim (PAS) domain, are essential and sufficient for the Pr → Pfr conversion (8). A ''read-out''

module, which in a still unknown manner interacts with the chromophore-binding domain, is linked to the specific function of the photoreceptor. In many bacterial phytochromes, this module is a histidine kinase function which shares similarities to the signaling domain of plant phytochromes although the biological function of the bacterial proteins is still enigmatic.

Bacterial and plant phytochromes bind different tetrapyrrole cofactors. Whereas the latter proteins bind a phytochromobilin (PΦB) and in very few cases of algal phytochromes also phycocyanobilin (PCB), or biliverdin IXα (BV) are the dominant chromophores in bacterial phytochromes (Fig. 1) (5,8). In all phytochromes, the bilin is covalently attached via its ring *A* ethylidene (PΦB, PCB) or vinyl (BV) side chain to a cysteine residue of the protein. The position of this cysteine, however, is different in the BV-binding and the PΦB/PCB-binding species (9). In plants, PΦB is covalently linked to a cysteine in the GAF domain (Cys-321 in phyA of oat), and a very similar chromophore-binding domain is found in the PCB-binding bacterial phytochromes. This residue, however, is missing in the BV-binding phytochromes that instead bind the BV chromophore via a cysteine residue located in the very N-terminal part of the protein. As an example, phytochrome from *Deinococcus radiodurans* (DrBphP), which has been crystallized as a truncated fragment (PAS-GAF domain), binds BV at Cys-24 (10). Despite the different binding sites and different types of chromophores, the bacterial phytochromes studied so far display a similar
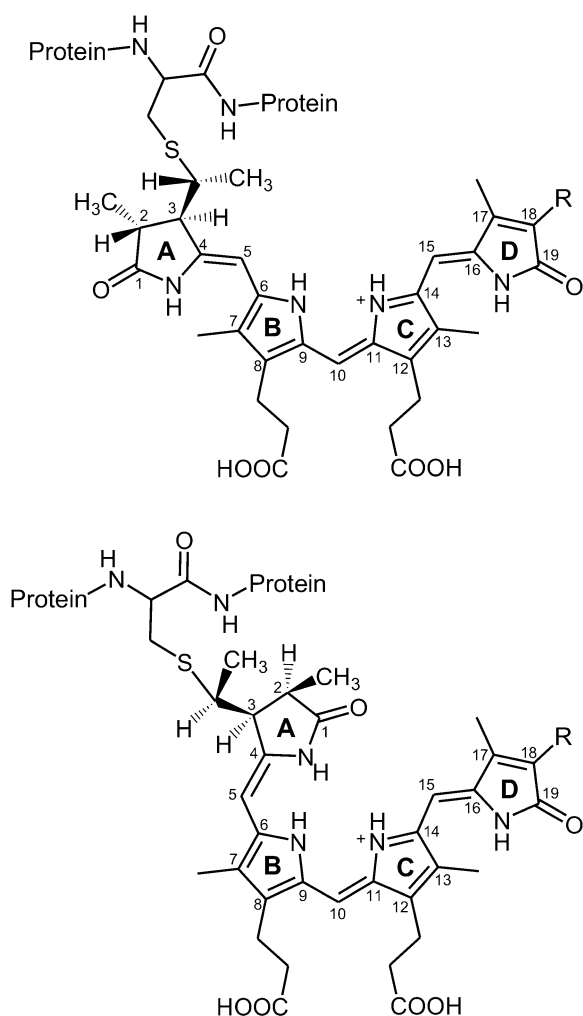
FIGURE 1 Structural formula for PΦB and PCB in the *ZZZasa* (*top*) and *ZZZssa* (*bottom*) configurations. R denotes the vinyl and ethyl substituent in PΦB and PCB, respectively.

Pr state. The results showed that only the calculated spectra of the *ZZZasa* geometry with the chromophore in a protonated (cationic) state (Fig. 1) provide a good reproduction of the experimental spectra. However, this analysis did not take into account the *ZZZssa* configuration, which has been identified as the chromophore structure in the Pr state of DrBphP.

This work is directed to resolve the apparent contradiction between the crystallographic and spectroscopic results. The comparison of the experimental and calculated vibrational spectra for phyA adducts reconstituted with different isotopically labeled chromophores indicates a *ZZZasa* configuration for the chromophore in the Pr state of plant phytochromes in contrast to the *ZZZssa* chromophore geometry in the Pr state of BV-binding phytochromes.

MATERIALS AND METHODS

Syntheses

15-D-PCB was synthesized as described by Knipp et al. (13). 5-^{13}C-PCB was synthesized according to Makhynya et al. (14). The synthesis followed the convergent strategy by generating the right and the left half of PCB separately (Fig. 1), followed by condensation of both compounds at the central C(10) position. 2-^{13}C-bromoacetic acid served as the isotope-labeled compound that was condensed to the α-(5-)position of ring *B*. Isotope content at position C(5) of the target PCB was >95% as determined by mass spectrometry.

Protein expression, purification, and reconstitution

5-^{13}C-PCB was assembled in a 5:1 molar ratio with recombinant his-tagged apo-phyA 65 of oat, spanning positions 1–595 of the full-length protein. The heterologous expression of the 65-kDa fragment of phyA has been described by Mozley et al. (15). The adducts obtained with PCB showed absorption maxima at 650 and 715 nm for Pr and Pfr, respectively. The isotopic labeling had no effect on the absorption maxima, the photochemical behavior, and the thermal stability.

Resonance Raman spectroscopy

RR spectra of the Pr state of phyA were obtained with 1064-nm excitation (neodymium-doped yttrium aluminum garnet continuous wave laser, line width <1 cm^{-1}) with Digilab Bio-Rad (Varian, Darmstadt, Germany) or a Bruker (Bruker Optics, Ettlingen, Germany) RFS 100/S Fourier transform Raman spectrometer (4 cm^{-1} spectral resolution). All spectra were measured at −140°C using a liquid nitrogen cooled cryostat (Linkam, Waterfield, Surrey, UK). The laser power was ~400 mW at the sample, which does not cause any laser-induced damage of the protein samples as checked by comparing the spectra obtained before and after a series of measurements. The total accumulation time was ~2 h for each spectrum. In all RR spectra shown in this work, the background was subtracted. Only for the phyA adduct reconstituted with C(15)-D PCB was the spectral quality relatively poor due to the low amount of the isotopomer that was available. Further experimental details have been described previously (16,17).

Quantum chemical calculations

Vibrational spectra were calculated by DFT using the B3LYP (three-parameter exchange functional according to Becke, Lee, Yang, and Parr (18)

reaction behavior, specifically for the sequence of intermediates and the reaction kinetics of the Pr → Pfr conversion (11,12). Thus, the bacterial phytochromes have been considered as model systems for the photoreceptors of plants.

In this respect, the recent determination of the three-dimensional structure of the Pr state of a phytochrome deletion mutant from DrBphP is of particular importance (10). Quite unexpectedly, the crystal structure reveals a *ZZZssa* configuration for the BV chromophore (Fig. 1), which is in contrast to the conclusions drawn from resonance Raman (RR) spectroscopic studies on plant phytochrome. In a previous work, the experimental RR spectra of the Pr state of phyA were compared with spectra calculated by density functional theory (DFT) for different chromophore geometries (6,7). The calculated geometries comprised more than 20 tetrapyrrole structures with different methine bridge configurations and conformations and also include those suggested previously for the chromophore geometry of the

and the 6–31G* basis sets except for Cl, for which the 6–31+G* basis set was adopted. All spectra refer to protonated (cationic) tetrapyrroles with a chloride ion in the vicinity of the pyrrole N-H groups serving as a counterion. The force field was scaled by a set of global scaling factors that have been previously determined for a series of model compounds (18) and further optimized for the ethylenic C-H out-of-plane coordinates (19) and the N-H coordinates of hydrogen-bonded systems (20). Further details of the computational methods are given elsewhere (19,20).

RESULTS AND DISCUSSION

The RR spectroscopic studies were carried out with the N-terminal 65-kDa fragment of phyA phytochrome, which exhibits the same spectral and kinetic properties as the full-length wild-type protein (21). Specifically, the RR spectra of the parent states and intermediates are identical, indicating that the truncation at the C-terminus does not affect the structure of the chromophore and its direct protein environment. The 65-kDa fragment of phyA can be reconstituted either with its natural chromophore PΦB or with PCB. Both adducts run through the photoinduced reaction cycle via the same intermediate states and with similar reaction kinetics. Due to the lack of the conjugated vinyl substituent at the D-ring in PCB, the absorption maxima of Pr and Pfr are hypsochromically shifted by ~15 nm in the PCB adduct as compared to phyA reconstituted with PΦB. The differences in the RR spectra are restricted to a few modes (vide infra), demonstrating that both chromophores adopt the same geometry in the respective states.

RR spectra of phyA reconstituted with PCB and PΦB

Fig. 2 shows the RR spectrum of the Pr state of the PCB adduct, phyA(PCB), in H_2O together with the calculated Raman spectra obtained for the ZZZssa and ZZZasa geometries. Taking into account the semiquantitative prediction of the Raman intensities and that the accuracy of the calculated frequencies is ~±10 cm^{-1} (18,19), the calculated Raman spectra of both geometries appear to describe the experimental spectrum equally well. The good correlation between the main experimental and calculated bands is outlined by the vertical dotted lines. Evidently, a decision about the most probable geometry of the Pr chromophore in phyA is not possible solely based on the comparison with the RR spectrum of phyA(PCB) even though a closer inspection of the various spectral regions reveals a better agreement for the ZZZasa configuration. Calculations of various ZZZasa conformers indicate that pyrrole side-chain conformations have a significant impact on the modes in the region below 1000 cm^{-1} (6), which in addition are expected to respond to dihedral distortions of the tetrapyrroles. This fine structure of the chromophore, however, is strongly influenced by the interactions with the protein environment, which cannot be mimicked by the quantum chemical calculations of the tetrapyrroles. On the other hand, conformational changes of
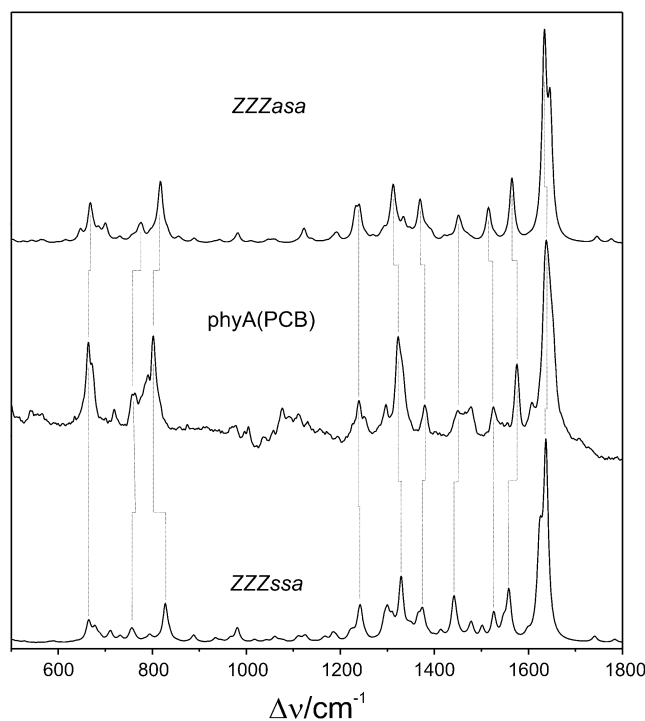

FIGURE 2 Calculated Raman spectra of protonated PCB in the ZZZasa (top: PCB, ZZZasa) and ZZZasa configuration (bottom: PCB, ZZZssa), compared with the experimental RR spectrum of the Pr state of 65-kDa phyA, reconstituted with PCB and measured in H_2O (middle: phyA(PCB)).

the pyrrole side chains do not affect the spectrum at higher wave numbers, specifically between 1500 and 1700 cm^{-1}. This region, which is dominated by modes involving the methine bridge stretchings, is expected to sensitively reflect different methine bridge geometries as shown by previous calculations of various Z/E (configuration of the methine bridge double bond) and s/a (conformation of the methine bridge single bonds) methine bridge isomers (6). This part of the spectrum will be, therefore, analyzed in more detail below.

The most prominent spectral difference between the experimental RR spectra of the Pr state of phyA(PΦB) and phyA(PCB) is in fact observed in the high-frequency region and refers to the strongest RR band in the experimental spectra, which shifts up from 1624 cm^{-1} in phyA(PΦB) to 1637 cm^{-1} in phyA(PCB) (Fig. 3; Table 1). Except for this frequency shift, the spectra of both adducts are very similar and only subtle differences are noted in the region below 800 cm^{-1} (19). Thus, it can safely be concluded that i) PCB adopts the same structure as PΦB upon incorporation in phyA, and (ii) the spectral changes between phyA(PΦB) and phyA(PCB) exclusively result from the different ring D substituents in PΦB (vinyl) and PCB (ethyl) (Fig. 1).

To rationalize these spectral changes we compare these experimental spectra with the spectra calculated for the ZZZssa and ZZZasa configurations (Fig. 3; Table 1). In both
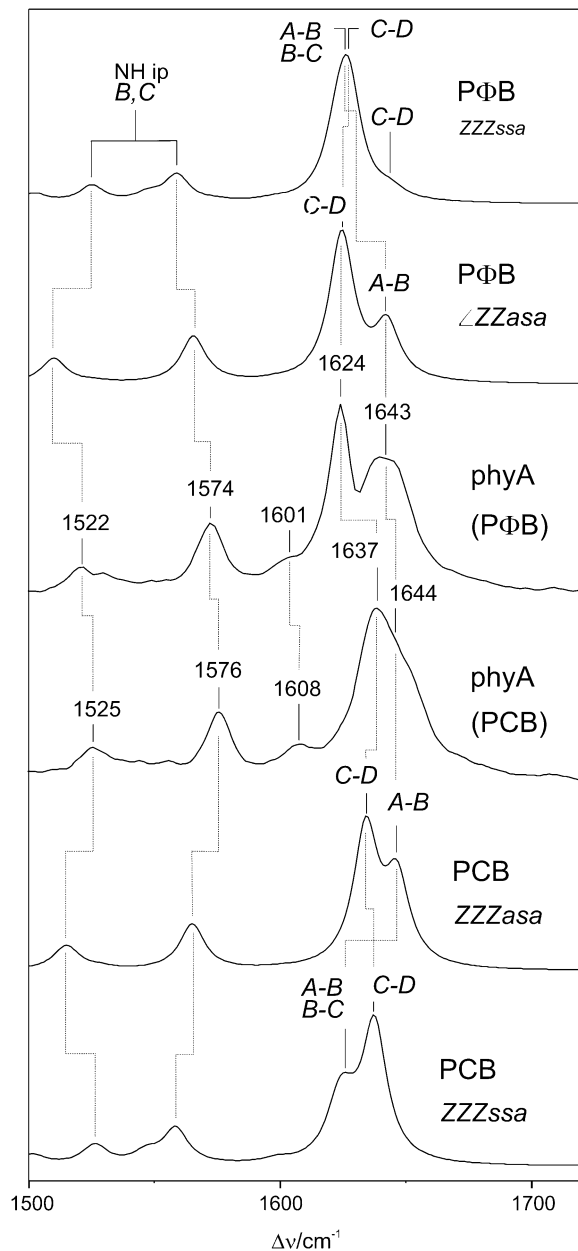
FIGURE 3 Calculated Raman spectra of protonated *ZZZssa* and *ZZZasa* configurations of PΦB and PCB (*top*: PΦB, *ZZZssa* and PΦB, *ZZZasa*; *bottom*: PCB, *ZZZasa* and PCB, *ZZZssa*), compared with the experimental RR spectra of the Pr state of 65-kDa phyA, reconstituted with PΦB and PCB and measured in H_2O (*middle*: phyA(PΦB) and phyA(PCB)).

cases, the strongest Raman activity is calculated for the mode dominated by the C=C stretching of the *C-D* methine bridge (*C-D* stretching) at 1625 and 1627 cm^{-1} in the *ZZZasa* and *ZZZssa* configuration of PΦB, respectively. Furthermore, a medium Raman intensity is predicted for the modes involving the C=C stretching of the *A-B* methine bridge (*A-B* stretching), which, however, are calculated at quite different frequencies for the *syn* and *anti* conformation. In the latter case (*ZZZasa*), this coordinate represents the main contribution to two closely

spaced modes at 1642 and 1643 cm^{-1}. In the spectrum calculated for the *ZZZssa* configuration the *A-B* stretching is mainly involved in one mode at 1623 cm^{-1}, which hence nearly coincides with the *C-D* stretching mode at 1627 cm^{-1}.

The experimental RR spectrum of phyA(PΦB) is dominated by the 1624-cm^{-1} band, which is well reproduced by the calculation of both geometries. However, the broad envelope centered at 1643 cm^{-1} indicates two overlapping medium-intense RR bands in the experimental spectrum, which is in good agreement with the prediction for the *ZZZasa* geometry. On the other hand, the calculated spectrum of the *ZZZssa* geometry shows only a single mode in this region (1644 cm^{-1}), which is localized in ring *D* and the adjacent methine bridge and exhibits only a weak Raman activity.

The replacement of the vinyl substituent at ring *D* in PΦB by an ethyl substituent in PCB has analogous effects on the calculated spectra of both geometries as far as the *C-D* stretching modes are concerned since they shift up by 9 cm^{-1} for both geometries, thereby reproducing the experimentally observed upshift of 13 cm^{-1}. Moreover, in the experimental RR spectrum the peak centered at 1637 cm^{-1} is much broader than its counterpart in phyA(PΦB), indicating the involvement of more than one RR band. In fact, for both configurations an additional medium-intense mode on the low-frequency side is calculated that mainly includes the C=C stretching of ring *D* (Table 1). However, only the calculations for the *ZZZasa* configuration yield an additional mode at 1644 cm^{-1}, which agrees very well with the shoulder on the high-frequency side of the 1637-cm^{-1} band. This mode is mainly composed of the *A-B* stretching. Conversely, for the *ZZZssa* configuration no mode is predicted in this region since the *A-B* stretching mode remains at nearly the same frequency (1622 cm^{-1}) as calculated for PΦB (1623 cm^{-1}) and thus constitutes a band pattern that does not match the experimental spectrum.

The region between 1520 and 1580 cm^{-1} further includes the protonation state marker bands originating from the N-H in-plane bending (N-H ip) of the inner pyrrole rings (17), which are found at very similar positions in the experimental RR spectra of phyA(PΦB) and phyA(PCB) (Fig. 3). For these modes, the frequencies calculated for the *ZZZasa* configuration are slightly lower than the experimental frequencies. This deviation can readily be understood since the frequencies of the N-H ip modes sensitively depend on the hydrogen-bond interactions with the protein that are not included in the calculation here (22). However, the separation of these modes ΔNHip appears to be independent of the hydrogen-bond interactions. In fact, the calculated mode separations for the *ZZZasa* configuration (55 and 53 cm^{-1} for PΦB and PCB, respectively) agree very well with the experimental values (51 cm^{-1} for phyA(PΦB) and phyA(PCB)), whereas the separations calculated for the *ZZZssa* geometry is distinctly smaller (34 and 35 cm^{-1} for PΦB and PCB, respectively) (Fig. 3; Table 1).

The calculations appear to underestimate the Raman intensities of the mode that is dominated by the *B-C* methine

TABLE 1 Experimental RR bands of phyA adducts and calculated normal modes for the *ZZZasa* and *ZZZssa* configurations of the chromophores

	Experimental RR bands of phyA(PΦB)										
ν, I	1646, s	1640, s	1624, vs		1601, w	1574, m		1526, w			1522, w
Calculated normal modes for the ZZZasa configuration of PΦB											
ν, I	1643, s	1642, m	1625, vs		1599, vw	1575, -	1565, m	1527, vw	1518, -	1510, w	
PED	30 A-B	27 A-B	23 C-D		51 B-C	47 ring D	28 N-H ip, B	31 ring B	11 ring B	13 N-H ip, B	
	15 vinyl	19 vinyl	29 vinyl		14 CH B-C	15 vinyl str	29 N-H ip, C		29 ring C	19 N-H ip, C	
Calculated normal modes for the ZZZssa configuration of PΦB											
ν, I	1644, w		1627, vs	1623, s	1597, vw	1574, -	1559, m	1547, w	1502, w	1525, m	
PED	38 C-D		38 C-D	22 A-B	19 B-C	50 ring D	26 N-H ip, B	31 ring B	46 ring C	18 N-H ip, C	
	14 vinyl		14 vinyl	15 B-C	16 ring B	16 vinyl str	21 N-H ip, C				
				12 ring B							
Experimental RR bands of phyA(PCB)											
ν, I [n.a.]	1644, s		1637, vs	1625, m	1608, w		1576, m	1525, w			
ν, I [C(15)-D]	1644, s		1624, vs				1570, m				
ν, I [C(5)-^{13}C]	~1629, m		1635, vs		1606, w		1573, m	1522, w			
Calculated normal modes for the ZZZasa configuration of PCB											
ν, I [n.a.]	1644, s		1634, vs	1629, m	1602, vw		1567, m	1525, w	1516, w	1514, m	
PED [n.a.]	58 A-B		57 C-D	68 ring D	49 B-C		29 N-H ip, B	33 ring C	32 ring B	16 N-H ip, B	
			12 CH C-D		18 CH B-C		32 N-H ip, C			21 N-H ip, C	
ν, I [C(15)-D]	1644, s		1619, vs	1628, m	1611, vw		1566, m	1523, w	1515, vw	1513, m	
ν, I [C(5)-^{13}C]	1622, m		1634, vs	1629, m	1600, w		1566, m	1525, w	1516, w	1513, m	
Calculated normal modes for the ZZZssa configuration of PCB											
ν, I [n.a.]			1636, vs	1627, m	1622, s	1596, w	1558, m	1545, m		1523, m	1501, w
PED [n.a.]			57 C-D	18 ring D	18 A-B	18 ring B	29 N-H ip, B	26 ring B		12 N-H ip, B	46 ring C
			10 CH C-D		35 B-C	23 A-B	32 N-H ip, C			16 N-H ip, C	
					12 CH B-C						
ν, I [C(15)-D]			1619, vs	1627, w	1624, m	1596, w	1558, m	1545, w		1522, w	1497, w
ν, I [C(5)-^{13}C]			1636, vs	1627, m	1617, m	1586, w	1556, m	1540, w		1521, m	1501, w

Abbreviations: frequencies (ν) are given in cm⁻¹, and relative band intensities (I) are classified qualitatively (vs, very strong; s, strong; m, medium; w, weak; vw, very weak). The normal mode compositions are given terms of the PED (in %), restricting to coordinates with a PED of more than 10%. *A-B*, *B-C*, and *C-D* refer to the stretching coordinates of the *A-B*, *B-C*, and *C-D* methine bridges, respectively. Further abbreviations are C-H *C-D*, C-H *B-C*; C-H in-plane bending of the *C-D* and *B-C* methine bridge hydrogens; ring *B*, ring *C*, ring *D*, C=C stretchings of the respective pyrrole rings; N-H ip *B*, N-H ip *C*, N-H in-plane bending of the N-H group in ring *B* and *C*, respectively; vinyl, C=C stretching of the vinyl substituent of ring *D*.

bridge stretching. This deficiency is evidently related to the errors in the calculated normal mode compositions. For PΦB, the *B-C* stretching mode is calculated with a very low intensity (∼1% of the *C-D* stretching) at 1599 and 1597 cm⁻¹ for the *ZZZasa* and the *ZZZssa* geometry, respectively. In the experimental RR spectrum a weak but clearly detectable band is observed at 1601 cm⁻¹ that shifts up to 1608 cm⁻¹ in phyA(PCB). This observation is consistent with the IR difference spectra for phyA(PΦB) and phyA(PCB), in which the *C-B* stretching mode gives rise to the most intense chromophore bands, in agreement with the calculations (P. Schwinté, unpublished results). However, only the spectra calculated for the *ZZZasa* configuration reveal a frequency upshift (+3 cm⁻¹), whereas for the *ZZZssa* geometry a slight downshift (−1 cm⁻¹) is predicted.

RR spectra of phyA reconstituted with PCB isotopomers

The comparison of the experimental and calculated spectra for the two phyA adducts strongly suggests that the 1637- and 1644-cm⁻¹ bands in the experimental spectrum of phyA(PCB) originate from the *C-D* and *A-B* stretching, respectively. To further check this conclusion we have, therefore, extended the studies to phyA(PCB) adducts with isotopically labeled chromophores which are expected to lead to selective shifts of the two modes. Deuteration at the *C-D* methine bridge [C(15)-D] causes a 13-cm⁻¹ downshift of the 1637-cm⁻¹ band in the experimental RR spectrum, whereas the highest-frequency band at 1644 cm⁻¹ remains unchanged and thus becomes better resolved and clearly detectable despite the poor signal/noise ratio (Fig. 4; Table 1). This pattern is nicely reproduced by the spectrum calculated for the *ZZZasa* configuration, whereas in the case of the *ZZZssa* configuration the highest-frequency mode shifts down to coincide with the C=C stretching of the *A-B* bridge.

The ^{13}C-substitution at the *A-B* bridge causes a frequency downshift of the most prominent peak by 2 cm⁻¹ in the experimental RR spectrum accompanied by a distinct intensity decrease at 1644 cm⁻¹ (Fig. 5; Table 1). Again, these findings can readily be rationalized by the Raman spectra calculated for the *ZZZasa* configuration since only the *A-B*

stretching is predicted to undergo a frequency downshift by 22 to 1624 cm^{-1}, whereas the C-D stretching (1634 cm^{-1}) and the adjacent ring D mode (1629 cm^{-1}) remain unchanged. As a consequence of the resultant close frequency spacing, the three modes lead to strongly overlapping bands in the calculated spectrum ($ZZZasa$) such that the envelope maximum shifts to a lower frequency and the intensity on the high-frequency side of the peak is reduced. The good reproduction of the experimental isotope effects can be better visualized by comparing the difference spectra (''natural abundance'' minus ''$^{13}C(5)$''). The deviations in the relative amplitudes and shapes of the signals are due to the arbitrarily chosen band profiles and line widths as well as to errors in the intensity calculations. These errors may be somewhat larger for closely spaced modes, as in the case of the $^{13}C(5)$-labeled tetrapyrrole (Table 1), due to increased uncertainties in the calculated normal mode compositions. Nevertheless, the difference spectrum derived from the calculations for the $ZZZasa$ geometry provides a distinctly better description of the experimental difference spectrum than the calculations for the $ZZZssa$ configuration.

CONCLUSIONS

The comparison of the experimental and calculated spectra of the various phyA adducts demonstrates that the methine-bridge stretching modes between 1580 and 1650 cm^{-1} constitute the most sensitive spectral markers for the methine-bridge configuration and conformation. In this respect, the spectra calculated for the $ZZZasa$ configuration provides the best description of the experimental spectra and specifically of the spectral changes brought about by altering the ring D substitution and by isotopic labeling. Further support for this assignment comes from the analysis of the RR spectrum of Lumi-R, which is formed from the Pr state by a $Z \rightarrow E$ photoisomerization of the C-D bridge (23). It has been shown that the experimental spectrum of Lumi-R of phyA is well reproduced by the calculations for the $ZZEasa$ but not by the $ZZEssa$ configuration (6).

The quantum chemical spectra calculations provide a frequency accuracy of ± 10 cm^{-1}, and RR intensities are predicted in a semiquantitative manner (18,19). Isotopic effects as well as the spectral changes brought about by the change of the ring D substituents should be reproduced even more accurately since systematic errors may partially cancel. Accordingly, the assignment of the chromophore structure for the Pr state of phyA to the $ZZZasa$ geometry appears to be unambiguous. This conclusion, however, is based on calculations that refer to the chromophore structure in vacuo and relies on the fact that the A-B stretching mode is at ~ 1643 cm^{-1} in the $ZZZasa$ but at ~ 1623 cm^{-1} in the $ZZZssa$ configuration. We therefore have to ask if the protein environment might affect the validity of the interpretation. Specifically, one has to discuss if interactions with the protein might perturb the structure of a hypothetical $ZZZssa$
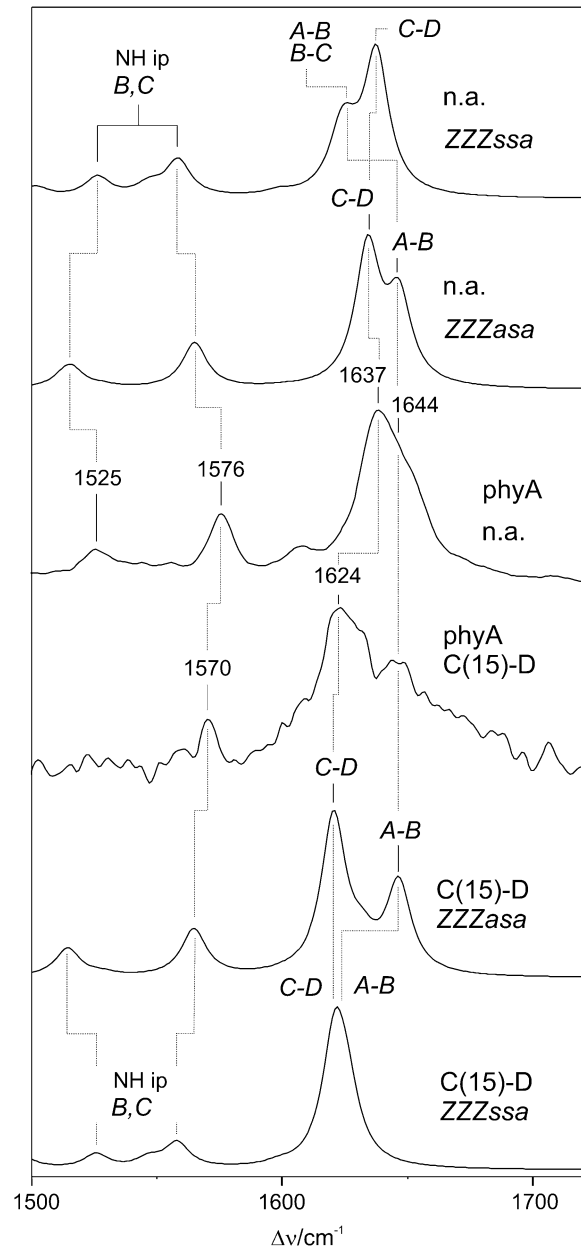

FIGURE 4 Calculated Raman spectra of the $ZZZssa$ and $ZZZasa$ configurations of protonated, unlabeled (natural abundance, na) PCB (*top*: n.a., $ZZZssa$ and n.a., $ZZZasa$) and protonated PCB deuterated at the methine bridge C-D [C(15)-D] (*bottom*: C15-D, $ZZZasa$ and C15-D, $ZZZssa$) compared with the experimental RR spectra of the 65-kDa fragment of phyA reconstituted with the unlabeled and C(15)-D PCB measured in H_2O (*middle*: phyA(n.a.), and phyA(C15-D)).

chromophore such that the A-B stretching is upshifted by ~ 20 cm^{-1}, and the vibrational band pattern in this region agrees with that of the free $ZZZasa$ chromophore. In this context it is interesting to refer to recent quantum mechanics/molecular mechanics (QM/MM) calculations on the antenna protein α-C-phycocyanin (α-CPC) (22).

This protein includes a protonated PCB chromophore in the $ZZZasa$ configuration as revealed by the crystal structure
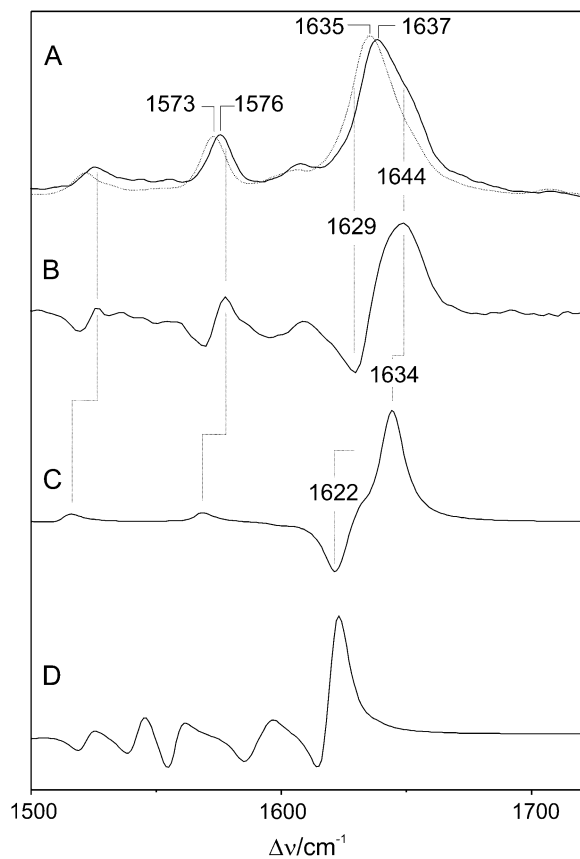
FIGURE 5 Experimental RR spectra of the Pr state of the 65-kDa fragment of phyA reconstituted with the (*A, solid line*) unlabeled and (*B, dotted line*) ^{13}C(5) PCB measured in H_2O. Trace *B* represents difference of the spectra in *A* (nonlabeled minus ^{13}C(5)). The corresponding difference spectra obtained from the calculated Raman spectra are shown in *C* (protonated *ZZZasa*) and *D* (protonated *ZZZssa*).

(24). According to the QM/MM calculations, which afford a better description of the experimental spectra than the quantum mechanical (QM) calculations, the *A-B* stretching shifts to a lower frequency and the *C-D* stretching thus exhibits the highest frequency in the C=C stretching region. Although this result shows that cofactor-protein interactions may in principle affect the methine bridge stretching modes, in phyA, the opposite frequency shift of this mode would be required to bring the calculated Raman spectrum of the *ZZZssa* geometry to coincide with the experimental spectrum. Hence, a hypothetical *ZZZssa* chromophore in the binding pocket of phyA had to be involved in interactions with the protein environment that are quite different as compared to DrBphP to produce a spectrum that is incidentally congruent with that of a *ZZZasa* chromophore calculated in vacuo and thus accounts for the experimental findings. Consequently, we conclude that the *ZZZasa* configuration represents the most likely chromophore structure for the Pr state in phyA.

This conclusion implies that the parent state of plant phytochromes adopts a different structure than DrBphP for

which the crystal structure has been determined (10). This difference may be related to the different location of the chromophore-binding Cys in the protein pocket. In fact, Agp1 phytochrome from *Agrobacterium tumefaciens*, which like DrBphP binds a BV via a Cys close to the N-terminus, also appears to adopt a *ZZZssa* chromophore structure in the Pr state (25). Regardless of the different chromophore structures in the Pr state, bacterial and plant phytochromes are likely to share a common reaction mechanism that is initiated by the $Z \rightarrow E$ isomerization at the *C-D* methine bridge, followed by chromophore and protein relaxation that includes a reversible deprotonation of the chromophore and the rotation around the *A-B* methine bridge (7).

REFERENCES

1. Schäfer, E., and F. Nagy, editors. 2006. Photomorphogenesis in Plants and Bacteria. Springer, Dordrecht, The Netherlands.

2. Rockwell, N. C., and J. C. Lagarias. 2006. The structure of phytochrome: a picture is worth a thousand spectra. *Plant Cell.* 18:4–14.

3. Rockwell, N. C., Y. S. Su, and J. C. Lagarias. 2006. Phytochrome structure and signaling mechanisms. *Annu. Rev. Plant Biol.* 57:837–858.

4. Kevei, E., and F. Nagy. 2003. Phytochrome controlled signalling cascades in higher plants. *Physiol. Plant.* 117:305–313.

5. Karniol, B., J. R. Wagner, J. M. Walker, and R. D. Vierstra. 2005. Phylogenetic analysis of the phytochrome superfamily reveals distinct microbial subfamilies of photoreceptors. *Biochem. J.* 392:103–116.

6. Mroginski, M. A., D. H. Murgida, and P. Hildebrandt. 2007. The chromophore structural changes during the photocycle of phytochrome: a combined resonance Raman and quantum chemical approach. *Acc. Chem. Res.* 40:258–266.

7. Mroginski, M. A., D. H. Murgida, D. von Stetten, C. Kneip, F. Mark, and P. Hildebrandt. 2004. Determination of the chromophore structures in the photoinduced reaction cycle of phytochrome. *J. Am. Chem. Soc.* 126:16734–16735.

8. Sharda, S., R. Shah, and W. Gärtner. 2007. Domain interaction in cyanobacterial phytochromes as a prerequisite for spectral integrity. *Eur. Biophys. J.* In press.

9. Lamparter, T., N. Michael, O. Caspani, T. Miyata, K. Shirai, and K. Inomata. 2003. Biliverdin binds covalently to *Agrobacterium* phytochrome Agp1 via its ring *A* vinyl side chain. *J. Biol. Chem.* 278:33786–33792.

10. Wagner, J. R., J. S. Brunzelle, K. T. Forest, and R. D. Vierstra. 2005. A light-sensing knot revealed by the structure of the chromophore-binding domain of phytochrome. *Nature.* 438:325–331.

11. Lamparter, T., F. Mittmann, W. Gärtner, T. Börner, E. Hartmann, and J. Hughes. 1997. Characterization of recombinant phytochrome from the cyanobacterium *Synechocystis*. *Proc. Natl. Acad. Sci. USA.* 94:11792–11797.

12. Remberg, A., I. Lindner, T. Lamparter, J. Hughes, C. Kneip, P. Hildebrandt, S. E. Braslavsky, W. Gärtner, and K. Schaffner. 1997. Raman spectroscopic and light-induced kinetic characterization of a recombinant phytochrome of the cyanobacterium Synechocystis. *Biochemistry.* 36:13389–13395.

13. Knipp, B., K. Kneip, J. Matysik, W. Gärtner, P. Hildebrandt, S. E. Braslavsky, and K. Schaffner. 1997. Synthesis and resonance Raman spectroscopic characterization of biliverdin and phycocyanobilin isotopomers. *Chem. Eur. J.* 3:363–367.

14 Makhynya, Y., Z. Hussain, T. Bauschlicher, P. Schwinté, F. Siebert, and W. Gärtner. 2007. Synthesis of selectively ^{13}C-labelled bilin compounds. *Eur. J. Org. Chem.* 8:1287–1293

15. Mozley, D., A. Remberg, and W. Gärtner. 1997. Large scale generation of affinity-purified recombinant phytochrome chromopeptide. *Photochem. Photobiol.* 686:710–715.

16. Kneip, C., P. Hildebrandt, W. Schlamann, S. E. Braslavsky, F. Mark, and K. Schaffner. 1999. Protonation state and structural changes of the tetrapyrrole chromophore during the $P_r \rightarrow P_{fr}$ phototransformation of phytochrome. A resonance Raman spectroscopic study. *Biochemistry.* 38:15185–15192.

17. von Stetten, D., S. Seibeck, N. Michael, P. Scheerer, M. A. Mroginski, D. H. Murgida, N. Krauss, M. P. Heyn, P. Hildebrandt, B. Borucki, and T. Lamparter. 2007. Highly conserved residues D197 and H250 in Agp1 phytochrome control the proton affinity of the chromophore and Pfr formation. *J. Biol. Chem.* 282:2116–2123.

18. Magdó, I., K. Nemeth, F. Mark, P. Hildebrandt, and K. Schaffner. 1999. Calculation of vibrational spectra of linear tetrapyrroles. 1. Global sets of scaling factors for force fields derived by ab initio and density functional theory. *J. Phys. Chem. A.* 103:289–303.

19. Mroginski, M. A., D. H. Murgida, and P. Hildebrandt. 2006. Calculation of vibrational spectra of linear tetrapyrroles. 4. Methine bridge C-H out-of-plane modes. *J. Phys. Chem. A.* 110:10564–10574.

20. Mroginski, M. A., K. Nemeth, T. Bauschlicher, W. Klotzbücher, R. Goddard, O. Heinemann, P. Hildebrandt, and F. Mark. 2005. Calculation of vibrational spectra of linear tetrapyrroles. 3. Hydrogen-bonded hexamethylpyrromethene dimers. *J. Phys. Chem. A.* 109:2139–2150.

21. Schmidt, P., T. Gensch, A. Remberg, W. Gärtner, S. E. Braslavsky, and K. Schaffner. 1998. The complexity of the Pr $\rightarrow$ Pfr photo-transformation kinetics is an intrinsic property of homogeneous native phytochrome. *Photochem. Photobiol.* 68:754–761.

22. Mroginski, M. A., F. Mark, W. Thiel, and P. Hildebrandt. 2007. QM/MM calculation of the Raman spectra of the phycocyanobilin chromophore in α-C-phycocyanin. *Biophys. J.* In press.

23. Rüdiger, W., F. Thümmler, E. Cmiel, and S. Schneider. 1983. Chromophore structure of the physiologically active form (Pfr) of phytochrome. *Proc. Natl. Acad. Sci. USA.* 80:6244–6248.

24. Schirmer, T., W. Bode, and R. Huber. 1987. Refined three-dimensional structures of two cyanobacterial C-phycocyanins at 2.1 and 2.5 Å resolution. *J. Mol. Biol.* 196:677–695.

25. Borucki, B., D. von Stetten, S. Seibeck, T. Lamparter, N. Michael, M. A. Mroginski, H. Otto, D. H. Murgida, M. P. Heyn, and P. Hildebrandt. 2005. Light-induced proton release of phytochrome is coupled to the transient deprotonation of the tetrapyrrole chromophore. *J. Biol. Chem.* 280:34358–34364.